Journal of Thermal Analysis and Calorimetry (2023) 148:12455–12466
https://doi.org/10.1007/s10973-023-12546-x

Environmentally friendly poly(butylene adipate-co-terephthalate) and CO_2-based poly(propylene carbonate) biodegradable foams modified with short basalt fiber

Hanlin Tian[1,2] · Jinshuo Yu[1,2] · Yan Zhao[1] · Hongwei Pan[1] · Yi Li[4] · Yang Xiao[4] · Lijing Han[1] · Junjia Bian[1] · Yanping Hao[3] · Huiliang Zhang[1,2]

Received: 29 April 2023 / Accepted: 27 August 2023 / Published online: 28 September 2023

Abstract

As environmental pollution continues to rise, the demand for biodegradable materials, particularly biodegradable foams, is steadily increasing. We prepared high-density foam using extended poly(butylene adipate-co-terephthalate) (E-PBAT) and poly(propylene carbonate) (PPC), with basalt fiber (BF) serving as the filler, through an extrusion process. We conducted a detailed study to investigate the impact of PPC and BF content on the foaming of E-PBAT. We conducted a detailed study on how PPC and BF content influence the foaming of E-PBAT. This investigation revealed the formation of various phase morphologies within the composites, including "island-sea," "quasi-co-continuous," and "co-continuous" structures, which, in turn, altered the cellular morphology. The BF network played a crucial role as a structural backbone, enhancing the composite material's modulus, yield strength, and rheological complex viscosity ($|\eta^*|$). Additionally, fiber networks can also serve as nucleation sites to promote cell nucleation and increase cell density. A higher cell density allows for more effective force transfer when the foam experiences external pressures, thereby enhancing its mechanical properties. We also summarized the mechanisms behind the changes in phase structure and fiber content on cell morphology. This summary provides valuable guidance for research on the extrusion foaming of biodegradable materials.

Keywords Poly(butylene adipate-co-terephthalate) · Poly(propylene carbonate) · Basalt fiber · Foam

Introduction

Polymer foams find extensive applications in various fields, particularly in packaging materials, owing to their exceptional attributes such as lightweight, specific strength, heat insulation properties, and sound isolation capabilities. Nonetheless, as foam waste accumulates and poses an environmental threat, there is a growing urgency to identify effective alternatives to conventional materials [1–3].

With the widespread use of biodegradable materials in the market, promising alternatives to traditional plastics have emerged. PBAT, a copolymer comprising a rigid BT segment (butylene terephthalate) and a flexible BA segment (butylene adipate) with excellent ductility and biodegradability [4], offers a compelling option. PBAT foams exhibit properties similar to those of traditional polyethylene (LDPE) foam, including sound and thermal insulation. This makes them a potential replacement for LDPE foam in applications such as packaging, biomedical, and automotive industries [5–7]. Another noteworthy biodegradable polymer is Poly(propylene carbonate) (PPC), synthesized from propylene oxide and carbon dioxide, offering excellent processing capabilities in methods like blown film, compression molding, injection molding, and extrusion casting [8–10]. Guan et al. conducted a study on the impact of the blowing agent (N, N′-dinitroso pentamethylene tetramine (DPT)) ratio on PPC foaming. It was found that DPT had a

✉ Hongwei Pan
hwpan@ciac.ac.cn

1 Key Laboratory of Polymer Ecomaterials, Chinese Academy of Sciences, Changchun Institute of Applied Chemistry, Changchun 130022, People's Republic of China

2 Changchun University of Technology, Changchun 130012, People's Republic of China

3 Shandong Dawn Polymer Co., Ltd, Longkou 265700, People's Republic of China

4 COFCO (Jilin) Bio-Chemical Technology Co., Ltd, Changchun 130033, People's Republic of China

chain-expanding effect on PPC, resulting in excellent foaming when the DPT content ratio ranged from 2 to 3 mass% [11].

PBAT and PPC blends have been the subject of extensive research. Pan et al. conducted a study in which they prepared PBAT and PPC blend blowing film. They observed a significant increase in tear strength, both in the machine direction (MD) and transverse direction (TD), with an increasing PPC content. Additionally, the gas barrier properties also saw a significant improvement [12]. In a separate study, Ma et al. incorporated PPC and nanosilica as reinforcing materials into PBAT. They discovered that this resulted in the formation of a double percolation structure in PBAT/PPC (70/30) blends. This structural change led to a reduction in the droplet size of PPC and a significant enhancement in the storage modulus and Young's modulus of the blends [13]. Due to PPC's unique structure and its exceptional CO2 adsorption capacity, Liu et al. successfully created PBAT/PPC foam. This foam exhibited a foaming ratio of 15 times when subjected to high-pressure CO2 and the ADR-4368 chain extender [9].

Compared to single polymer, composites exhibit a variety of foaming behaviors depending on the interfacial interaction and phase structure [14]. Fiber is natural or artificially oriented material that is often used as fillers in polymer. What is more, the difference in content and distribution of fiber in the matrix has an impact on the melt strength, crystallinity, and interfacial interaction, which affect the foaming behavior [15]. An investigation had shown that, when maple fiber was added into polyurethane foam, the cell distribution was more uniform and cell size became larger. Interestingly, due to the addition of fibers in the synthesis process, a network structure will be formed in the polymer chain, resulting in the obstruction of chain joint movement and the increase of T_g [16]. Wang et al. used castor oil as matrix to prepare biodegradable foams by adding short sisal fibers. And the effects of fiber length, fiber content and alkali or silane coupling agent on foam properties were summarized [17]. A study of physical foaming of poly(lactic acid) (PLA)/pulp fiber composite was described by Rokkonen et al. [18]. Isobutane blowing agents were found to have a smoother foam surface than CO_2 blowing agents, and the pulp fibers helped to reduce cell size and inhibit prone rupturing and coalescing. In Kuang's study [19], polytetrafluoroethylene (PTFE) powder was added to PPC and poly (butylene succinate) (PBS) blends to produce composite foam and was processed into fibrous filaments by the shearing action of the screw extruder, thereby enhancing the mechanical properties and foaming capacity. The same phenomenon was confirmed by Peng's research [20], where the formation of a network of PTFE fibers led to significant improvements in the rheological and mechanical properties of the polymer.

Basalt fiber (BF) originates from solidified lava from basalt-based volcanic rocks [21]. As an inorganic fiber material, BF distinguishes itself not only for its cost-effectiveness compared to carbon fiber but also for its superior mechanical properties when compared to E-glass fiber. When used as a filler, BF finds extensive application in polymer materials due to its high modulus, exceptional strength, and excellent thermal stability [22, 23]. Kurańska et al. were pioneers in incorporating low-cost BF waste into polyurethane (PU) foam, resulting in significant enhancements in thermal properties, thermo-mechanical stability, and curing strength. This approach to recycling industrial waste is environmentally friendly [24]. In another study, Wang et al. introduced short BF into Polyether-Ether-Ketone (PEEK) to create composites. These composites exhibited an impressive specific wear rate, with the lowest value recorded at 25% BF content, measuring 5.28×10^{-7} m^3 N^{-1} m^{-1} [25]. Pan et al. made a noteworthy discovery concerning coupling agent-treated BF (SBF) and BF powder (SBFP). These materials not only acted as heterogeneous nucleating agents for PLA but also enhanced its mechanical properties. The impact strength of PLA/SBF/SBFP 50/30/20 reached 16.8 kJ m^{-2}, and the heat deflection temperature improved from 59 to 140 °C. Nonetheless, BF may indeed contribute to enhancing foaming properties and reinforcing foams.

In previous study, we investigated the foaming behavior of extended PBAT (E-PBAT)/PPC blends in relation to their composition by extrusion. Considering the effect the phase structure and complex viscosity on the foaming properties of the blends, the structure of cells changed noticeably, but the density of cells was not expected [26]. BF is not commonly used in polymer foaming due to its inert surface properties and high density. Nevertheless, this paper introduces BF into various PBAT/PPC blend ratios. The objective of this research is to investigate how the BF content affects the mechanical properties, thermal properties, viscosity, and cell structure of these blends. Ultimately, the aim is to present BF as a superior alternative to traditional foam materials.

Experimental

Materials

The PBAT (45%BA-co-55%BT) used in this experiment was supplied by Xinjiang Blue Ridge Tunhe Polyester Co, Ltd, and number average molecular weight (M_n) and polydispersity index (PDI) were 8.9×10^4 g mol^{-1} and 1.85, respectively. PPC was produced by Changchun Institute of Applied Chemistry, Chinese Academy of Sciences. The M_n and PDI of neat PPC determined by GPC were 3.0×10^5 g mol^{-1} and 2.1, respectively. The bis(tert-butyl dioxy isopropyl) benzene (BIBP) was supplied by

Dongguan Huan-zong Trading Co. Ltd. (Guangdong, China). The chemical foaming agent Azodicarbonamide (AC) was supplied by Shanghai Dingfen Chemical Technology Co, Ltd (AR grade, 97% purity). Short BF was supplied by Shenzhen Tianzhitu Co, Ltd. The length of BF was 6 mm, with a diameter of about 15 μm.

PBAT chain extension modification

PBAT was dried in an oven at 60 °C for 6 h before mixing to minimize the effect of moisture, then mixed with 0.2 mass% BIBP and added to the twin-screw extruder (SHJ-20, Lanzhou Lantai Plastics Machinery Engineering Co. Ltd, Lanzhou, China, $L/D = 20$) to obtain the E-PBAT, the extrusion temperature was 120–180 °C from the feed throat to the die for nine temperature range, and the rotor speed was 200 rad min^{-1}. E-PBAT was cooled in a water bath, cut into pellets and dried in an oven for 24 h before foaming.

Foaming process

E-PBAT, PPC, and BF were blended with 2 mass% AC foaming agent using a twin (single) screw extruder unit (Tianhua Chemical Machinery and Automation Research and Design Institute Co, Ltd, S(T)J-20/25) to prepare E-PBAT/PPC/BF foam. Table 1 shows the composition of the E-PBAT/PPC/BF foam. The processing temperature at 15 zones was independently in the range of 130–150 °C, the twin-screw speed was 200 rad min^{-1}, single-screw speed was 450 rad min^{-1}, the residence time was around 1.5 min, the input was 5 kg h^{-1}, and the output was 4.8 kg h^{-1}. The foaming process is shown in Fig. 1.

Table 1 The composition of the E-PBAT/PPC/BF foam composites

Samples (wt/wt/wt)	E-PBAT	PPC	BF
90/10/X	90	10	0
	90	10	1
	90	10	3
	90	10	5
	90	10	7
70/30/X	70	30	0
	70	30	1
	70	30	3
	70	30	5
	70	30	7
50/50/X	50	50	0
	50	50	1
	50	50	3
	50	50	5
	50	50	7

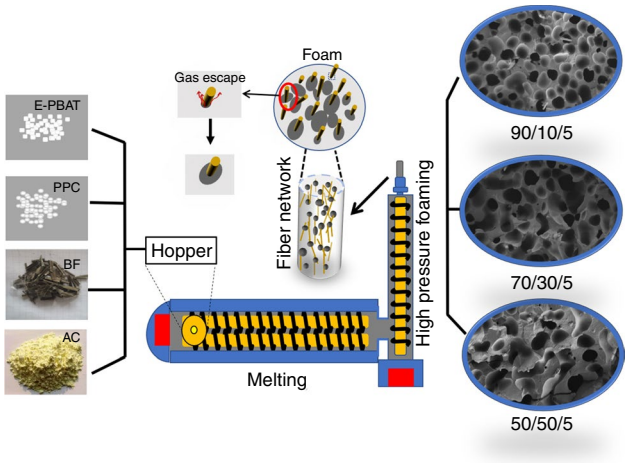

Fig. 1 Diagram of the foaming process

Characterizations

Rheological measurements

The rheological behavior of the samples was measured by a Physical MCR 2000 rheometer (TA Instruments AR2000ex, USA) equipped with parallel plates (25 mm in the diameter and 0.6 mm in gap) at 150 °C.

Tensile tests

The tensile tests were carried out on a universal testing machine (WSM-2KN, Changchun Intelligent Instrument and Equipment Co., Ltd., China), and dumbbell-shaped sample (20 mm × 4 mm × 1 mm) was cut from compression molded plate. The mechanical property parameters of the samples were tested at 20 °C and a cross-head speed of 20 mm min^{-1}. Five specimens of each sample were selected for testing and averaged.

Differential scanning calorimetry (DSC)

The thermal behaviors of E-PBAT/PPC/BF composites were studied by TA Instruments (DSC Q20 with a Universal Analysis 2000). The samples (5–8 mg) were filled and sealed in an aluminum tray, and the whole experiment process was under the protection of nitrogen atmosphere (flow rate of 50 mL min^{-1}). All samples were heated from -60 to 150 °C at a rate of 10 °C min^{-1} (first heating),

isothermal for 3 min, then cooled to -70 °C at a rate of 10 °C min^{-1} (first cooling), and finally heated to 150 °C at a rate of 10 °C min^{-1} again (second heating).

Dynamic mechanical analysis (DMA)

DMA experiment was used by a dynamic mechanical analyzer (DMA 850, TA USA) to characterize the relationship between the storage modulus and loss factor of the material and temperature. Amplitude and frequency were 5 μm and 1 Hz, and test temperature ranged from -60 to 80 °C at 3 °C min^{-1}.

Scanning electronic microscopy (SEM)

Both the morphology and cell structure of the foamed samples were observed using scanning electron microscope (SEM, Merlin, Zeiss, Merlin) at 1 kV accelerating voltage. A representative micrograph of greater than 50 bubbles was obtained as well as the cell density (N_o) and average cell area in the micrograph was determined by Image J. The results for each component were averaged over five samples and error bars were made. N_o, the number of cells per cubic centimeter of foaming samples was obtained by Eq. (1):

$$N_0 = \left[\frac{nM^2}{A}\right]^{3/2} \frac{\rho}{\rho_f} \quad (1)$$

where n is the number of cells in the SEM micrograph, M is the magnification factor, A is the area of the micrograph (cm^2), ρ and ρ_f are the mass densities of samples before and after foaming treatment.

Result and discussion

Melt rheology properties

Rheological analysis was considered as an effective method to evaluate the melt processing parameters, dispersion of fillers, filler-matrix interaction, and morphology in composites. Figure 2 represents the complex viscosity ($|\eta^*|$) and storage modulus (G') versus frequency for the E-PBAT/PPC/BF foam composites. From Fig. 2a–c, as the PPC content increased from 10, 30, and 50 mass%, the $|\eta^*|$ of the 90/10/X, 70/30/X, 50/50/X composites had an apparent increase attributed to higher melt strength of PPC. As the BF content increased from 1 to 7 mass%, $|\eta^*|$ of the 90/10/X, 70/30/X, and 50/50/X composites increased with increased shear frequency, and the reinforcement of BF was more obvious in the low-frequency range than in the high-frequency range. In high-frequency region, the fibers followed the flow effect of the polymer melt in terms of orientation, thus reducing interlayer interactions [27], indicating the formation of a BF network and the inhibitory effect of this network on chain relaxation [28]. The enhanced melt strength and elasticity would be beneficial to support the cell growth. The G' slightly increased with increasing BF content at frequencies ranging from 0.1 to 100 rad s^{-1}, all samples exhibited similar rheological curves, as shown in Fig. 2a′–c′, and possible reason may be that the fibers followed the flow effect of the polymer melt in terms of orientation.

Tensile mechanical properties

The tensile stress–strain curves for 90/10/X, 70/30/X, and 50/50/X composites are shown in Fig. 3a–c. The main mechanical properties are listed in Table 2. It was clear that both PBAT and PPC composites showed toughness fracture, while in 90/10/0, Young's modulus and yield strength were about 72.1 MPa and 7.2 MPa. However, the values increased significantly with increasing PPC and BF content. With increasing PPC content, the Young's modulus and yield strength of the composites increased to 210.9 MPa and 8.7 MPa of 50/50/0. The increase in BF in the composites also resulted in a significant increase in Young's modulus and yield strength, after addition 7 mass% BF, the Young's modulus increased by 98.7% and yield strength increased by 39.8% in the 90/10/X component. In addition, in the curves of the composites, the yield behavior was more obvious under the synergistic effect of phase structure and BF, and the maximum Young's modulus and yield strength of 278.1 MPa and 14.1 MPa were achieved in the 50/50/7 component. Furthermore, the yield strain of the composites exhibited a substantial increase as the BF content increased. The maximum increase observed ranged from 8.7 for the 50/50/0 blend to 14.2 for the 50/50/7 blend. This suggests that BF can effectively provide support for stresses before yielding °C curs. The increase in modulus and yield strength of composites may be due to the "island-sea", "quasi-co-continuous", and "co-continuous" phase structures, which were transferred from the matrix to BF when stressed, resulting in a uniform and effective stress distribution, leading to a significant increase in Young's modulus and yield strength of the composites [29, 30]. In addition, the formation of a fiber network supported the polymer matrix, leading to an increase in modulus and yield strength [31]. With increasing BF content, the elongation at break of the composites decreased, even was below 100%. Due to the different strain properties between BF and the polymer matrix, PBAT/PPC deforms under tensile stress, but the fibers were not, and when the tensile force was greater than the bond strength between the fibers and the matrix, interface debonding resulted in a reduction in elongation at break [13]. In

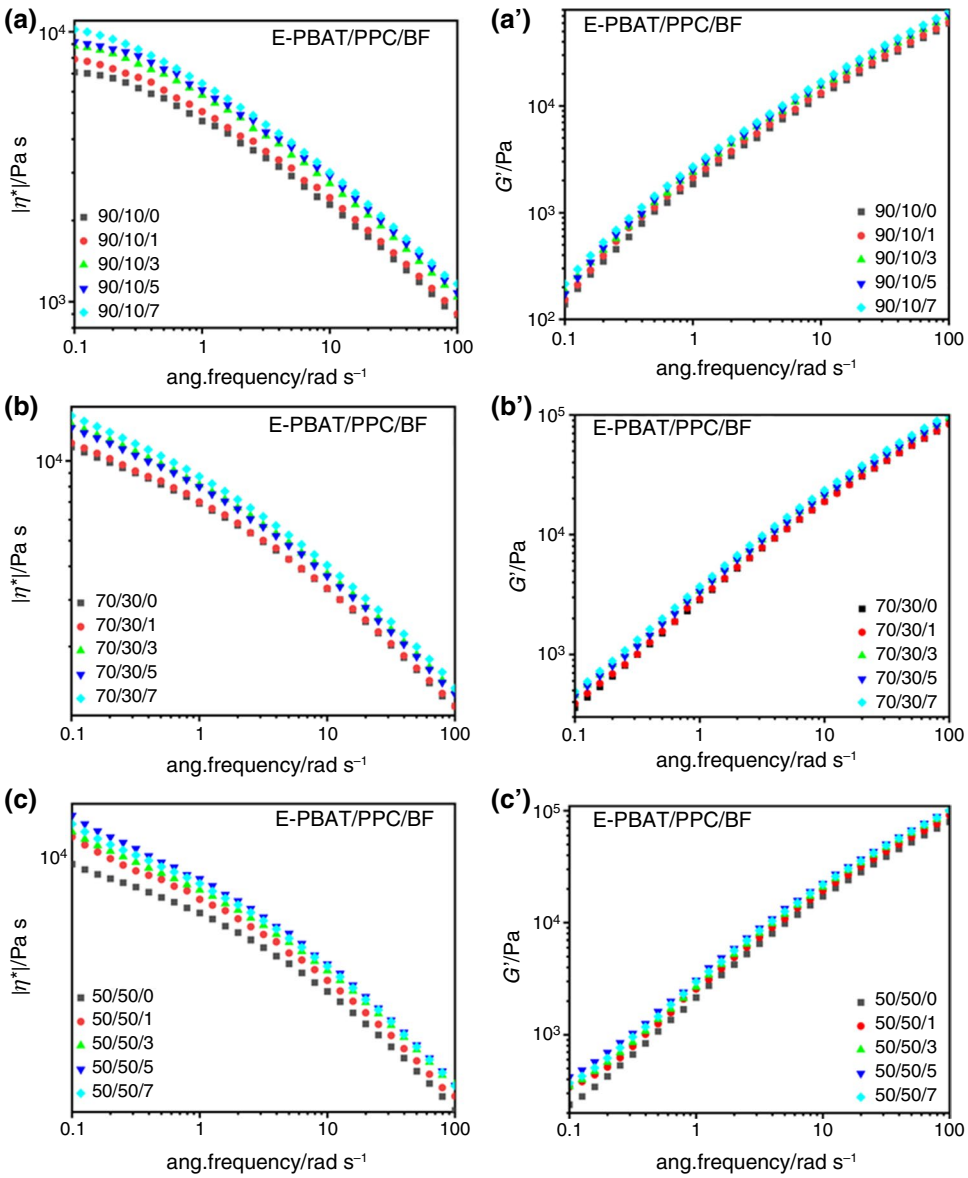

Fig. 2 Complex viscosity (|η*|) (**a**–**c**) and storage modulus (G') (**a**′–**c**′) curves versus frequency for 90/10/X, 70/30/X, and 50/50/X foam composites

addition to that, for discontinuous fiber-filled composites sometimes show ineffective reinforcement because of the subcritical length of the fiber and poor interaction between fibers and matrix. Although the elongation at break of the composites decreased as the components changed, in most cases it maintained a high modulus and stress.

Thermal behaviors

DSC was used to investigate the effect of the component on the thermal and crystalline properties. The second heating and cooling traces of E-PBAT/PPC and E-PBAT/PPC/BF composites were shown in Fig. 4a, b, respectively, and the corresponding data are listed in Table 3. The small peak at around -33 °C was T_g of PBAT. At the same time, PPC was an amorphous polymer with a glass transition temperature around 35 °C. It was worth nothing that the T_g of PBAT decreased from − 32.8 °C of 90/10/0 to − 34.7 °C of 50/50/0, while the T_g of PPC decreased from 36.1 to 31.0 °C. According to Gao et al. analysis [32], PPC had a "solvent" effect, penetrated into the molecules of PBAT and thus reducing the stacking density. However, the decreased in T_g of PPC may be attributed to free volume effect [12]. From the crystallinity data, it becomes evident that an increase in PPC content results in a decrease in the crystallinity of PBAT. This phenomenon is likely due to the amorphous phase of PPC becoming embedded in the PBAT molecular chain, thereby restricting the formation of crystalline regions. Additionally, the weak crystallization capacity of PBAT, coupled with the influence of fibers on crystallization, leads to a decline in crystallinity. This decline is more pronounced and influenced by the fiber network content. During the foaming

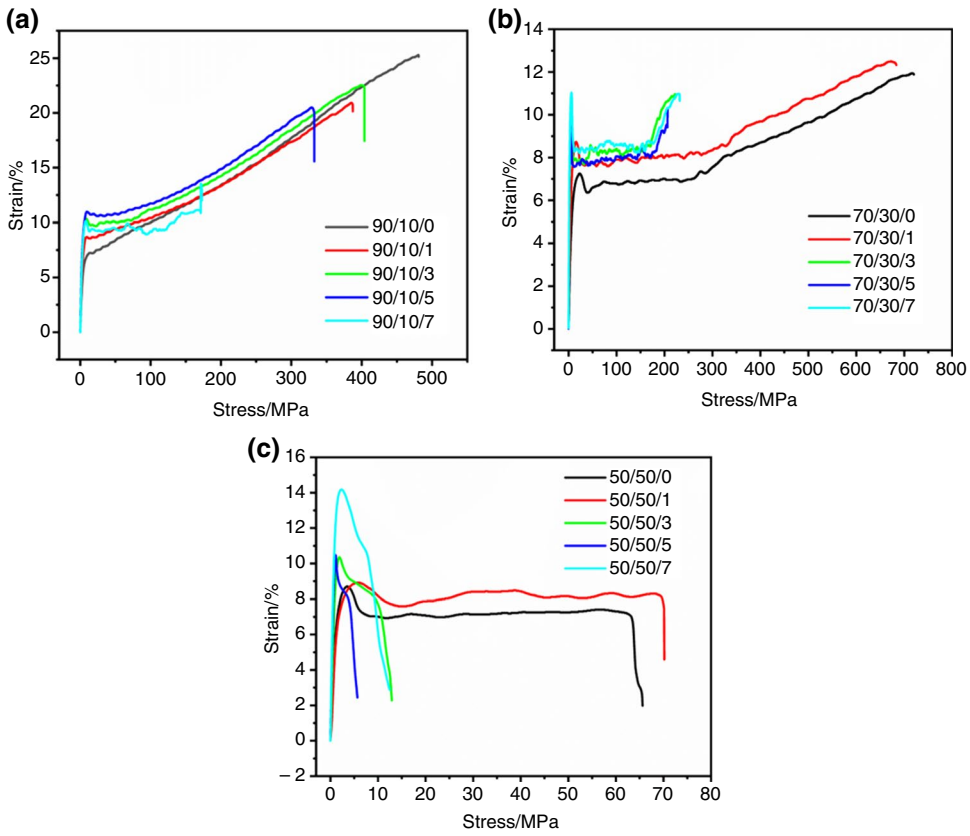

Fig. 3 Tensile stress–strain curves for **a** 90/10/X, **b** 70/30/X, and **c** 50/50/X composites

Table 2 Tensile dates of 90/10/X, 70/30/X, and 50/50/X composites

Sample name	Young's modulus/MPa	Yield strength/MPa	Tensile strength/MPa	Elongation at break/%	Yield strain/%
90/10/0	72.1 ± 10.2	7.2 ± 0.6	25.2 ± 3.2	480.9 ± 55.7	7.2 ± 0.9
90/10/1	80.8 ± 12.3	8.6 ± 0.7	20.9 ± 2.8	387.3 ± 32.8	8.7 ± 0.8
90/10/3	113.1 ± 13.5	10.3 ± 0.9	22.5 ± 2.5	403.8 ± 37.6	10.1 ± 0.7
90/10/5	139.1 ± 17.0	10.9 ± 0.9	20.4 ± 2.2	332.6 ± 28.0	10.3 ± 0.6
90/10/7	143.3 ± 19.8	10.1 ± 0.8	11.1 ± 0.9	171.1 ± 20.1	11.0 ± 0.9
70/30/0	138.1 ± 17.6	7.2 ± 0.6	11.9 ± 1.1	719.9 ± 68.9	7.2 ± 0.7
70/30/1	159.3 ± 17.5	8.7 ± 0.8	12.5 ± 1.1	718.1 ± 70.8	8.7 ± 0.8
70/30/3	185.9 ± 19.5	9.8 ± 0.9	10.9 ± 0.8	223.9 ± 20.2	9.3 ± 0.8
70/30/5	205.0 ± 21.2	11.0 ± 1.1	11.0 ± 1.0	231.8 ± 20.1	9.9 ± 0.7
70/30/7	217.7 ± 21.1	9.4 ± 0.8	9.5 ± 0.9	206.1 ± 19.9	11 ± 0.6
50/50/0	210.9 ± 21.6	8.7 ± 0.67	8.7 ± 0.8	65.6 ± 67.2	8.7 ± 0.4
50/50/1	228.7 ± 22.3	11.1 ± 1.1	11.1 ± 1.0	76.6 ± 7.1	8.9 ± 0.7
50/50/3	240.1 ± 24.2	10.3 ± 0.9	10.3 ± 1.0	12.9 ± 1.1	10.3 ± 0.5
50/50/5	263.8 ± 25.5	10.4 ± 1.0	10.4 ± 0.8	5.7 ± 0.4	10.5 ± 0.4
50/50/7	278.1 ± 25.2	14.1 ± 1.2	14.1 ± 1.1	12.5 ± 1.8	14.2 ± 0.8

process, the lamellae of the polymer crystalline structure impede the diffusion of gas to the external environment [33]. Conversely, a reduction in crystallinity enhances the gas escape rate.

Dynamic mechanical properties

Dynamic mechanical analysis (DMA) was apparent response of the storage modulus (E'), which was a measurement of the stiffness of the materials, as well as for the T_g (the tanδ peak).

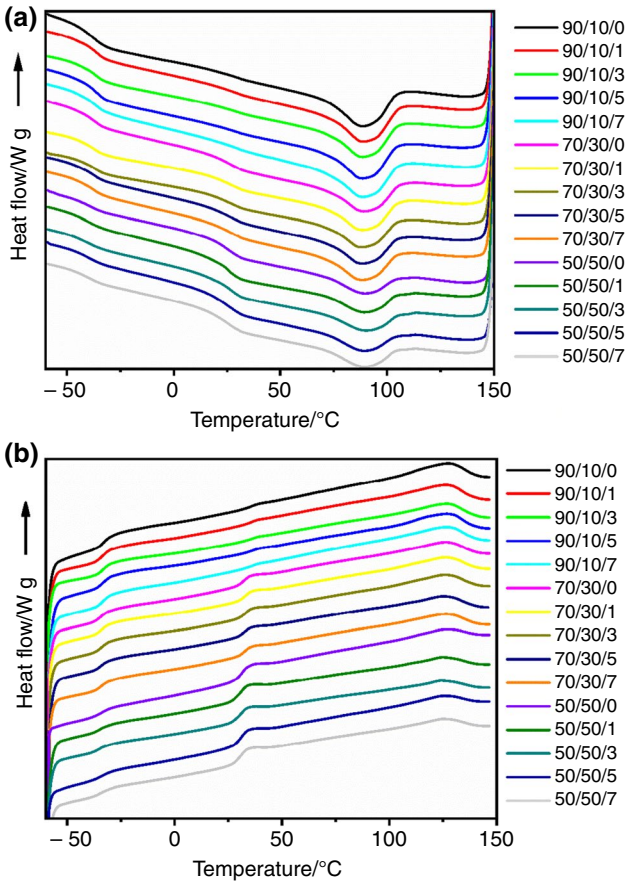

Fig. 4 cooling trace (**a**) and Second heating trace (**b**) of DSC curves for composites

Figure 5a–c shows the curves of E' of 90/10/X, 70/30/X, and 50/50/X composites, respectively. The decreasing step about -30 °C was featured the glass transition of PBAT, whereas a broad decreasing step about 35 °C was related to the glass transition of PPC. The values of E' of the composites were influenced by the PPC and BF, and the increase in fibers can effectively improve the thermal stability of PPC. For example, at 60.0 °C, it was found that E' of the 90/10/X sample increased from 30.5 to 54.0 MPa, 70/30/X sample increased from 20.6 to 53.7 MPa, and 50/50/X sample increased from 12.5 to 49.6 MPa, increased by 77%, 160%, and 297%, respectively, indicating that the formation of fiber network improved the stiffness of composite [34] and the fibers being more likely to synergy with higher melt strength of PPC and increased the stiffness of the foam products [35]. The introduction of BF significantly improved the tensile yield strength and DMA hardness of composites, which improves the range of use of the material. Tanδ was used to measure the compatibility of the E-PBAT/PPC composites. Figure 5a′–c′ presents tanδ curves of the E-PBAT/PPC/BF composites. For E-PBAT/PPC/BF composites, tanδ curves revealed two T_g values, where the higher T_g corresponded to PPC and the lower T_g corresponded to PBAT. The appearance of two T_g values correspond to immiscibility of each individual component. The T_g of PBAT in 90/10/X shifted toward lower temperature with increasing BF content (Fig. 5a′), and the result was consistent with DSC. The T_g of PBAT and PPC in 70/30/X was almost unchanged with increasing BF content (Fig. 5b′). The T_g of PPC in 50/50/X increased slightly around 35–40 °C for the glass transition.

Table 3 Thermal and crystalline properties of composites from DSC curves

E-PBAT/PPC/BF	T_{g1}/°C	T_{g2}/°C	T_m/°C	ΔH_m/J g^{-1}	T_c/°C	χ_c/%
90/10/0	– 32.8	36.1	127.1	6.9	88.3	6.7
90/10/1	– 33.1	35.8	126.4	6.2	88.6	6.1
90/10/3	– 33.5	35.9	126.9	5.8	88.5	5.8
90/10/5	– 33.6	36.4	126.7	5.7	88.3	5.8
90/10/7	– 34.2	36.1	126.8	5.6	88.5	5.9
70/30/0	– 34.1	31.9	126.3	4.5	89.2	5.7
70/30/1	– 34.9	32.9	125.9	5.2	88.6	5.9
70/30/3	– 33.8	33.4	125.6	4.5	88.0	5.9
70/30/5	– 34.9	33.0	125.0	4.8	88.2	5.6
70/30/7	– 34.4	33.3	128.1	3.9	88.1	5.3
50/50/0	– 34.7	31.1	125.3	3.2	89.0	5.6
50/50/1	– 35.2	31.0	124.5	3.3	89.5	5.8
50/50/3	– 34.0	31.0	124.0	3.4	89.7	5.4
50/50/5	– 35.3	31.3	125.0	2.9	89.3	5.4
50/50/7	– 34.8	31.3	125.7	2.1	88.8	3.9

Melting temperature (T_m) and enthalpy (ΔH_m)

Degree of crystallinity, χ_c (%) = $\Delta H_m / W_{PBAT} \times \Delta H^0_m$ (ΔH^0_m, the melting enthalpy of 100% crystalline PBAT being taken as 114 J g^{-1}, W_{PBAT} is the mass fraction of PBAT in the blend.)

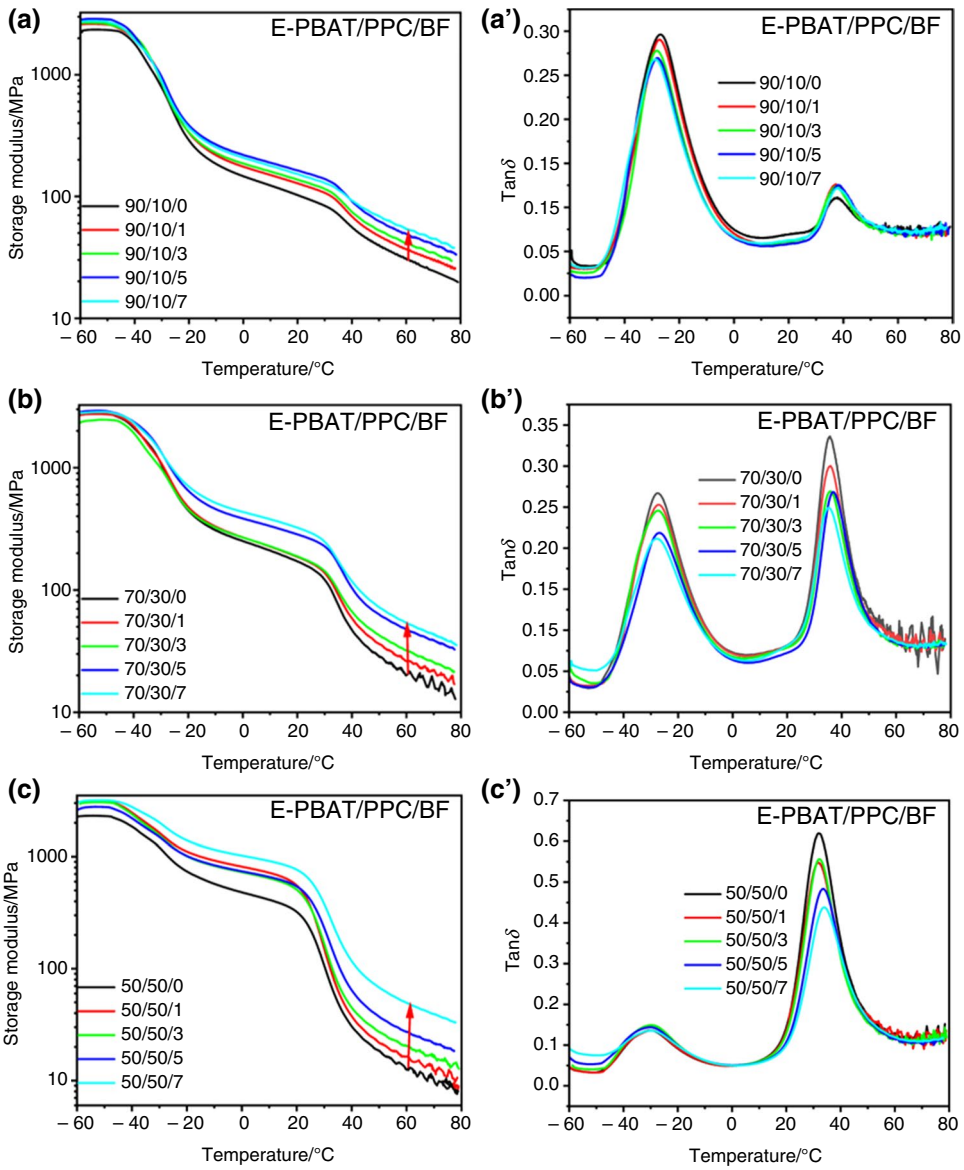

Fig. 5 Storage modulus (**a**) and tanδ (**b**) curve versus temperature for 90/10/X, 70/30/X, and 50/50/X foam composites

Foam behavior

The cell morphology of the foam and SEM images of BF embedded in E-PBAT and PPC are shown in Fig. 6, and the parameters of cell density, expansion ratio, and average cell size of E-PBAT/PPC/BF composites are presented in Fig. 7. From Fig. 6A, it was found that the cell density of 90/10/X sample increased significantly with increasing BF content, and the highest cell density and the largest expansion ratio were founded with 6.24×10^6 cells/cm^3 and 2.13 in 90/10/7 and 90/10/1. Wang et al. and Chen et al. demonstrated that the fibers were embedded in the matrix and acted as heterogeneous nucleation sites for the nucleation of bubbles, reducing the nucleation barrier described by classical bubble theory [36]. Figure 6B shows the fracture surface of E-PBAT/PPC/BF 70/30/X sample. In a previous study, we investigated the foaming behavior of E-PBAT/PPC blends in relation to their composition by extrusion, as the phase structure changed from 90/10 "sea-island" structure to 70/30 "quasi-continuous" structure, cell was easy to form on the interface of two phases [26]. After addition BF, the inorganic fibers promoted the deformation of cells. The nucleation mechanism of cells during extrusion can be explained as follows: Under the high-speed shear and high-temperature conditions of the extruder, the blowing agent was thermally decomposed to produce gas, and a large amount of gas was dissolved in polymer. When the foam was extruded, the pressure returned to atmospheric and the gas escaped from the polymer, producing the foam. Compared with neat blends, the blending of BF can reduce the surface free energy barriers which was beneficial to nucleation, so BF can improve the cell density and cell structure.

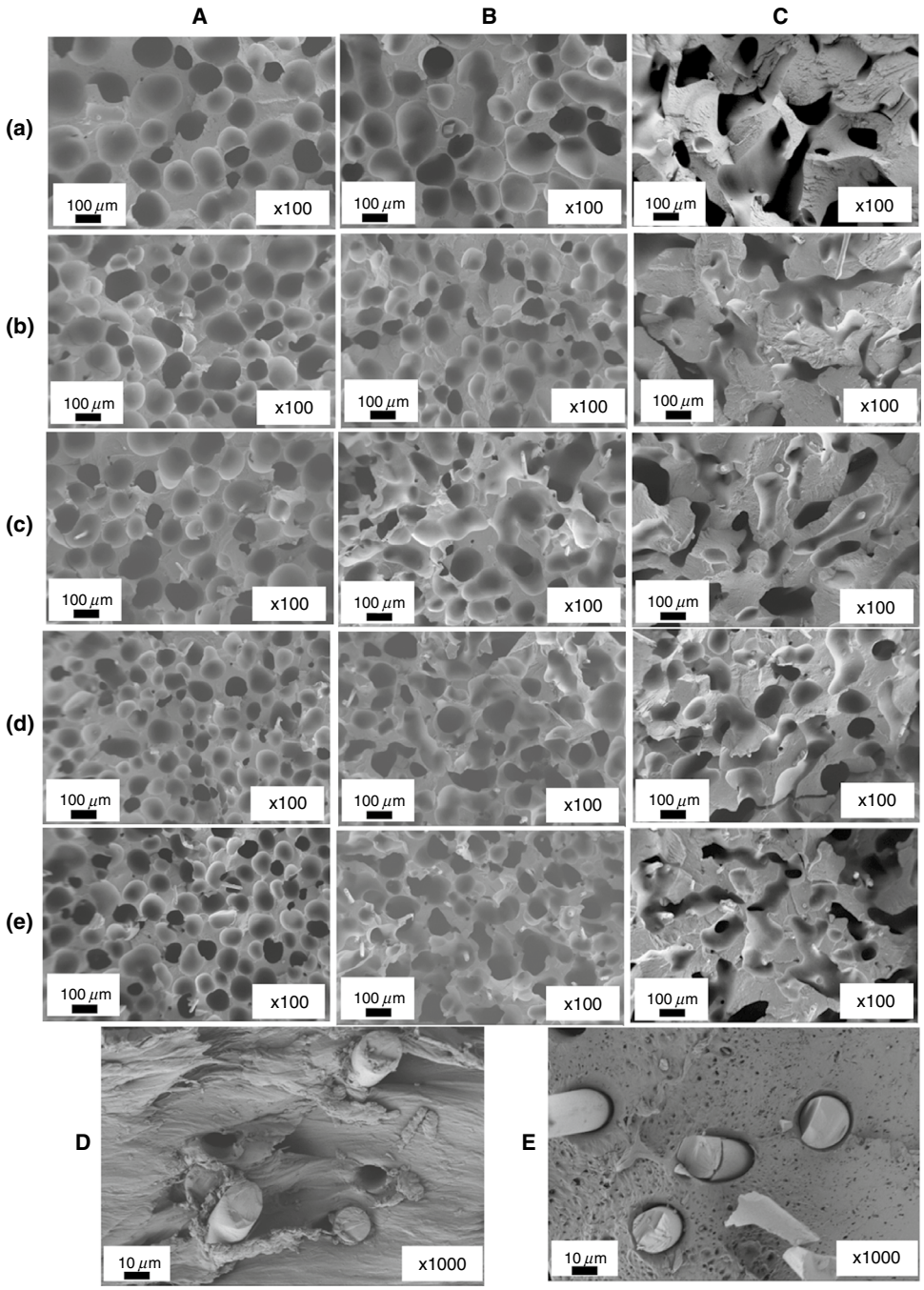

Fig. 6 The cell structure of different fiber contents in 90/10/X (**A**), 70/30/X (**B**), and 50/50/X (**C**) composites at 100 × magnification where (a)–(e) were BF contents of 0, 1, 3, 5 and 7 mass%, respectively, SEM images of BF embedded in E-PBAT (**D**) and PPC (**E**)

In the E-PBAT/PPC 50/50 component, as shown in C-(a), since PPC and PBAT were continuous phases with each other, the gases were more inclined to escape between the phase interfaces of the two polymers, resulting in a long strip-like cell structure. After addition fibers, the barrier to cell formation decreased, nucleate more easily, the cell size was significantly reduced and the cell structure became uniform. The interface ability of the fibers to the polymer matrix had a significant effect on the foaming behavior, the interface debonding between BF and PPC, which acted as a path for gas escape during the foaming process that promoted the growth and fixation of cells. As shown in C-(b) and (c), the average cell area of 50/50/X foam composites was much higher than those of the other two samples, which leaded to a lower cell density, but it was greatly improved after the addition of 5 mass% BF. Although 7 mass% BF given the highest density and minimum cell size, the excessive BF was uneven distributed at the interface, resulted in merging of cells, so 5 mass% BF works best. Taken together, the results of the above analyses demonstrate that BF significantly enhances

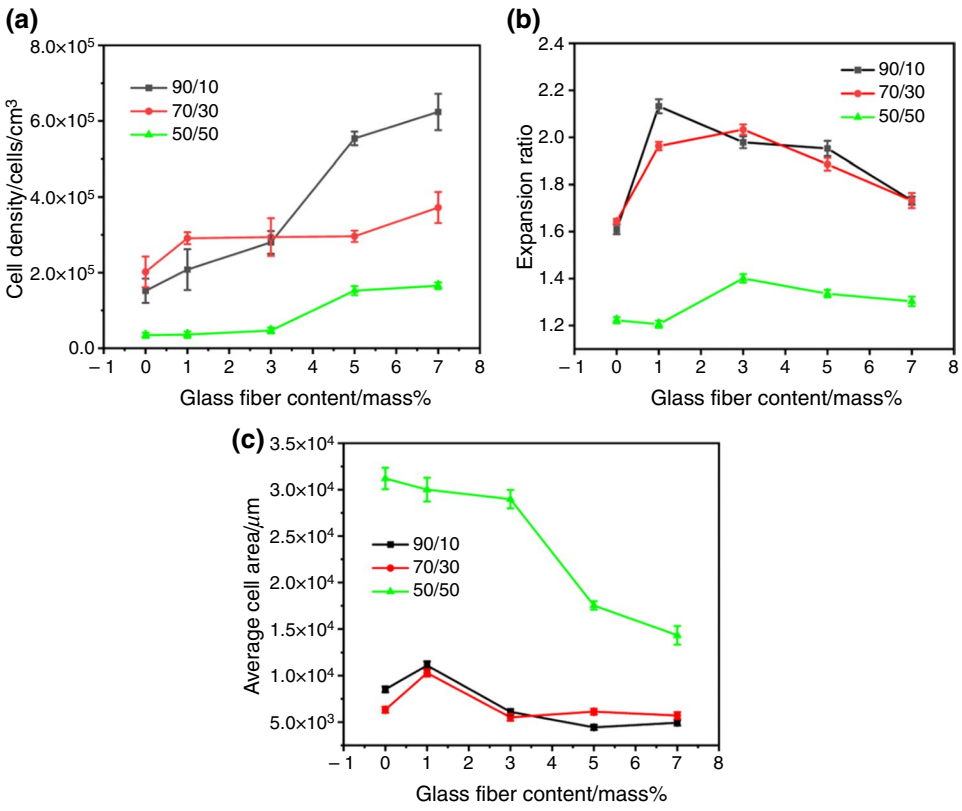

Fig. 7 **a** Cell density, **b** expansion ratio and **c** average cell area of E-PBAT/PPC/BF foam composites

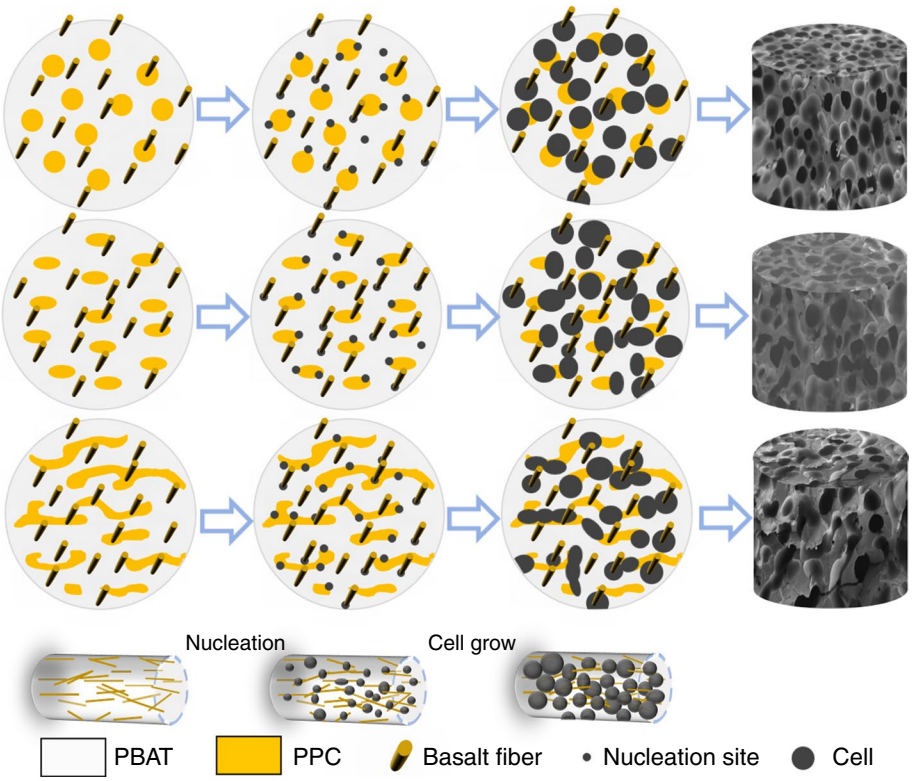

Fig. 8 Nucleation and foaming mechanism of E-PBAT/PPC/BF composites **a** E-PBAT/PPC/BF 90/10/5, **b** E-PBAT/PPC/BF 70/30/5, **c** E-PBAT/PPC/BF 50/10/5

the strength of the composites, including the modulus and yield strain before yielding, thereby expanding the potential applications of PBAT/PPC/BF foams.

Foaming mechanism

The difference in the rheological properties of the two polymers and fibers would induce two types of cellular morphology. Nucleation and foaming mechanism of E-PBAT/PPC/BF composites is shown in Fig. 8. E-PBAT/PPC foaming property was uniform, leading to the formation of good dispersion of cell in the matrix. When the BF added, BF was evenly distributed in the cell wall without obvious aggregation, indicating good dispersion of BF in the matrix. The nucleation sites were mainly located at the interface between the two phases and around the fibers. Accordingly, the formation of fiber networks and changed in phase structure had a significant effect on the morphology of cells.

Conclusions

In summary, the E-PBAT/PPC/BF foam composites were successfully prepared by extrusion. After addition fiber in polymer, the tensile modulus and strength of material increased significantly, with a maximum increase of 98.8% in 90/10/X, reaching a maximum tensile modulus and yield strength of 278.1 MPa and 14.1 MPa, respectively, in 50/50/7. The formation of the fiber network also had a significant effect on DMA storage modulus, with the maximum increase of 77%, 160% and 297%, respectively, at 60.0 °C. Due to the heterogeneous nucleation effect of the fibers, the cell density increased notably, which reaching the maximum of 6.24×10^6 cells/cm^3 in 90/10/7. The addition of 5 mass% BF also had a significant effect on cell structure of 50/50/X. This article will offer theoretical guidance for the application of biodegradable composite foam, making it a promising alternative for functions such as cushioning, filling, and cost reduction.

Acknowledgements This work was supported by the fund of the Science and Technology Bureau of Changchun City of China (No. 21SH13), Development and Reform commission of Jilin Province of China (2021C039-2), Science and Technology Bureau of Jilin Province of China (No. 20210509017RQ), Yantai science and technology innovation development plan project (2022ZDCX015), the Science and Technology Development Plan of Jilin Province (20210203199SF) and (20220203019SF).

Declarations

Conflict of interest The authors declare that they have no financial interests or personal relationships that could have appeared to influence the work reported in this paper.

References

1. Kahvand F, Fasihi M. Microstructure and physical properties of thermoplastic corn starch foams as influenced by polyvinyl alcohol and plasticizer contents. Int J Biol Macromol. 2020;157:359–67.
2. Li YT, Zhang ZY, Wang WM, Gong PJ, Yang Q, Park CB, Li GX. Ultra-fast degradable PBAT/PBS foams of high performance in compression and thermal insulation made from environment-friendly supercritical foaming. J Supercrit Fluids. 2022;181:105512.
3. Shi XT, Qin JB, Wang L, Ren LC, Rong F, Li DH, Wang R, Zhang GC. Introduction of stereocomplex crystallites of PLA for the solid and microcellular poly(lactide)/poly(butylene adipate-co-terephthalate) blends. RSC Adv. 2018;8(22):11850–61.
4. Kijchavengkul T, Auras R, Rubino M, Selke S, Ngouajio M, Fernandez RT. Biodegradation and hydrolysis rate of aliphatic aromatic polyester. Polym Degrad Stab. 2010;95(12):2641–7.
5. Arruda LC, Magaton M, Bretas RES, Ueki MM. Influence of chain extender on mechanical, thermal and morphological properties of blown films of PLA/PBAT blends. Polym Test. 2015;43:27–37.
6. Dou Q, Cai J. Investigation on polylactide (PLA)/poly(butylene adipate-co-terephthalate) (PBAT)/bark flour of plane tree (PF) eco-composites. Materials. 2016;9(5):393.
7. Nofar M, Heuzey MC, Carreau PJ, Kamal MR, Randal J. Coalescence in PLA- PBAT blends under shear flow: effects of blend preparation and PLA molecular weight. J Rheol. 2016;60(4):637–48.
8. Yang GH, Su JJ, Gao J, Hu X, Geng CZ, Fu Q. Fabrication of well-controlled porous foams of graphene oxide modified poly (propylene-carbonate) using supercritical carbon dioxide and its potential tissue engineering applications. J Supercrit Fluids. 2013;73:1–9.
9. Liu ZR, Hu JJ, Gao FX, Cao H, Zhou QH, Wang XH. Biodegradable and resilient poly (propylene carbonate) based foam from high pressure CO_2 foaming. Polym Degrad Stab. 2019;165:12–9.
10. Cai WR, Liu PJ, Bai SB, Li S. A one-step method to manufacture biodegradable poly (butylene adipate-co-terephthalate) bead foam parts. Polym Adv Technol. 2021;32(5):2007–19.
11. Guan LT, Du FG, Wang GZ, Chen YK, Xiao M, Wang SJ, Meng YZ. Foaming and chain extension of completely biodegradable poly(propylene carbonate) using DPT as blowing agent. J Polym Res. 2007;14(3):245–51.
12. Pan HW, Hao YP, Zhao Y, Lang XZ, Zhang Y, Wang Z, Zhang HL, Dong LS. Improved mechanical properties, barrier properties and degradation behavior of poly(butylenes adipate-co-terephthalate)/poly(propylene carbonate) films. Korean J Chem Eng. 2017;34(5):1294–304.
13. Ma YM, Gao FX, Zhang SL. Crystalline, rheological and mechanical enhancement in PBAT/PPC/silica nanocomposites with double percolation network. Chin J Polym Sci. 2022;40(11):1482–92.
14. Li Y, Cao CF, Li SN, Huang NJ, Mao M, Zhang JW, Wang PH, Guo KY, Gong LX, Zhang GD, Zhao L, Guan LZ, Wan YJ, Tang LC, Mai YW. In situ reactive self-assembly of a graphene oxide nano-coating in polymer foam materials with synergistic fire shielding properties. J Mater Chem A. 2019;7(47):27032–40.
15. Hou JH, Jiang J, Guo HY, Wang XF, Shen YQ, Li Q. Fabrication of fibrillated and interconnected porous poly(epsilon-caprolactone) vascular tissue engineering scaffolds by microcellular foaming and polymer leaching. RSC Adv. 2020;10(17):10055–66.
16. Gu RJ, Sain MM, Konar SK. A feasibility study of polyurethane composite foam with added hardwood pulp. Ind Crops Prod. 2013;42:273–9.

17. Wang HJ, Zhang CY, Rong MZ, Zhang MQ, Czigany T. Interfacial effects in short sisal fiber/maleated castor oil foam composites. Compos Interfaces. 2008;15(2–3):95–110.
18. Rokkonen T, Peltola H, Sandquist D. Foamability and viscosity behavior of extrusion foamed PLA–pulp fiber biocomposites. J Appl Polym Sci. 2019;136(41):48202.
19. Kuang TR, Li KC, Chen BY, Peng XF. Poly (propylene carbonate)-based in situ nanofibrillar biocomposites with enhanced miscibility, dynamic mechanical properties, rheological behavior and extrusion foaming ability. Compos Part B-Eng. 2017;123:112–23.
20. Peng XF, Li KC, Mi HY, Jing X, Chen BY. Excellent properties and extrusion foaming behavior of PPC/PS/PTFE composites with an in situ fibrillated PTFE nanofibrillar network. RSC Adv. 2016;6(4):3176–85.
21. Banibayat P, Patnaik A. Variability of mechanical properties of basalt fiber reinforced polymer bars manufactured by wet-layup method. Mater Des. 2014;56:898–906.
22. Dhand V, Mittal G, Rhee KY, Park SJ, Hui D. A short review on basalt fiber reinforced polymer composites. Compos B. 2015;73:166–80.
23. Wang X, Wu ZS, Wu G, Zhu H, Zen FX. Enhancement of basalt FRP by hybridization for long-span cable-stayed bridge. Compos Part B-Eng. 2013;44:184–92.
24. Kuranska M, Barczewski M, Uram K, Lewandowski K, Prociak A, Michalowski S. Basalt waste management in the production of highly effective porous polyurethane composites for thermal insulating applications. Polym Test. 2019;76:90–100.
25. Wang BW, Yu SD, Mao J, Wang YH, Li MJ, Li XP. Effect of basalt fiber on tribological and mechanical properties of polyether-ether-ketone (PEEK) composites. Compos Struct. 2021;266:113847.
26. Tian HL, Wang ZP, Jia SL, Pan HW, Han LJ, Bian JJ, Li Y, Yang HL, Zhang HL. Biodegradable foaming material of poly (butylene adipate-co-terephthalate)(PBAT)/poly (propylene carbonate) (PPC). Chin J Polym Sci. 2022;40(2):208–19.
27. Song JB, Liu JX, Zhang HL, Yang WB, Chen LH, Zhong YM, Ma CC. PVDF/PMMA/basalt fiber composites: morphology, melting and crystallization, structure, mechanical properties, and heat resistance. J Appl Polym Sci. 2014;131(13):40494.
28. Wang YQ, Mi JG, Du ZJ, Chen SH, Zhang C, Wang XD. Peculiar micro and nano cell morphology of PBT/PTFE nanofibrillated composite foams of supercritical CO_2 foaming induced by in-situ formed 3D PTFE nanofiber networks. Polymer. 2021;232:124165.
29. Huda MS, Drzal LT, Mohanty AK, Misra M. Chopped glass and recycled newspaper as reinforcement fibers in injection molded poly(lactic acid) (PLA) composites: a comparative study. Compos Sci Technol. 2006;66(11–12):1813–24.
30. Du WH, Zhang JT, Zhao ZX, Zhang X. Preparation of novel temperature-responsive double-network hydrogel reinforced with aramid nanofibers. Compos Commun. 2020;22:100438.
31. Zheng ZB, Wu HY, Si Y, Jia YT, Ding B. Stretchable and resilient fibrous sponges tailored by interlocking double-network for warmth retention. Compos Commun. 2021;27:100788.
32. Gao M, Ren ZJ, Yan SK, Sun JR, Chen XS. An Optical microscopy study on the phase structure of poly(L-lactide acid)/poly(propylene carbonate) blends. J Phys Chem B. 2012;116(32):9832–7.
33. Song JS, Mi JG, Zhou HF, Wang XD, Zhang YX. Chain extension of poly (butylene adipate-co-terephthalate) and its microcellular foaming behaviors. Polym Degrad Stab. 2018;157:143–52.
34. Wang GL, Zhang DM, Wan GP, Li B, Zhao GQ. Glass fiber reinforced PLA composite with enhanced mechanical properties, thermal behavior, and foaming ability. Polymer. 2019;181:121803.
35. Balachandrakurup V, Gopalakrishnan J. Enhanced performance of cellulose nanofibre reinforced styrene butadiene rubber nanocomposites modified with epoxidised natural rubber. Ind Crops Prod. 2022;183:114935.
36. Wang W, Han CY, Wang XH, Zhou GB, Xu MZ. Enhanced rheological properties and heat resistance of poly (propylene carbonate) composites with carbon fiber. Compos Commun. 2020;21:100422.